Engineering Analysis with Boundary Elements 37 (2013) 309–318

Contents lists available at SciVerse ScienceDirect

Engineering Analysis with Boundary Elements

journal homepage: www.elsevier.com/locate/enganabound

A low-frequency fast multipole boundary element method based on analytical integration of the hypersingular integral for 3D acoustic problems

Haijun Wu [a], Yijun Liu [b], Weikang Jiang [a,*]

[a] State Key Laboratory of Mechanical System and Vibration, Shanghai Jiao Tong University, Shanghai 200240, China
[b] Mechanical Engineering, University of Cincinnati, Cincinnati, Ohio 45221-0072, USA

ARTICLE INFO

Article history:
Received 24 February 2012
Accepted 25 September 2012

Keywords:
Boundary element method
Fast multipole method
Analytical singular integral
Acoustics

ABSTRACT

A low-frequency fast multipole boundary element method (FMBEM) for 3D acoustic problems is proposed in this paper. The FMBEM adopts the explicit integration of the hypersingular integral in the dual boundary integral equation (BIE) formulation which was developed recently by Matsumoto, Zheng et al. for boundary discretization with constant element. This explicit integration formulation is analytical in nature and cancels out the divergent terms in the limit process. But two types of regular line integrals remain which are usually evaluated numerically using Gaussian quadrature. For these two types of regular line integrals, an accurate and efficient analytical method to evaluate them is developed in the present paper that does not use the Gaussian quadrature. In addition, the numerical instability of the low-frequency FMBEM using the rotation, coaxial translation and rotation back (RCR) decomposing algorithm for higher frequency acoustic problems is reported in this paper. Numerical examples are presented to validate the FMBEM based on the analytical integration of the hypersingular integral. The diagonal form moment which has analytical expression is applied in the upward pass. The improved low-frequency FMBEM delivers an algorithm with efficiency between the low-frequency FMBEM based on the RCR and the diagonal form FMBEM, and can be used for acoustic problems analysis of higher frequency.

1. Introduction

The boundary element method (BEM) plays a dominant role in solving infinite or semi-infinite acoustic wave problems due to easy handling of boundary condition at infinity and dimension reduction. However, it suffers from well-known drawbacks with regard to the computational efficiency and memory requirement, because the conventional BEM leads to a linear system of equations with dense coefficient matrix. This prevents the conventional BEM from being applied to large-scale problems.

To overcome this problem, many studies have been conducted on the fast multipole method (FMM) accelerated BEM (FMBEM), one of the popular fast solution methods for the BEM. The FMM was first innovated by Rokhlin to rapidly calculate potentials of a large-scale particle system [1]. It was generalized by Greengard [2] to compute two-dimensional and three-dimensional Laplace equations in particle simulations. Later on, it was extended to 2D and 3D acoustic wave problem [3,4]. The efficiency of the FMBEM in acoustic analysis has been recognized gradually in acoustic community. Therefore the FMBEM has been extensively studied and widely used for acoustic problems since the end of the last century. The mathematical theory of multipole translation operators, one of underlying theory of low-frequency (LF) FMBEM for 3D Helmholtz equation, was summarized by Epton and Dembart [5]. The diagonal form translation operators and its error analysis was given by Rahola [6]. Methods to accelerate the LF FMBEM were proposed in Ref. [7,8] which replace the classical multipole expansion with a representation in term of evanescent waves and propagating waves. Sakuma and Yasuda employed the high-frequency (HF) FMBEM for large-scale steady-state sound field analysis in the series papers [9,10]. Two rough criteria to determine the number of cell levels which can minimize processing time and memory requirements respectively were proposed in Ref. [10]. Later on, they discussed an effective setting of the hierarchical cell structure [11], and developed a technique of plane-symmetric model [12] for FMBEM. Chen and Chen developed a FMBEM for 2D exterior acoustics based on dual integral formulation by adopting the addition theorem and expanding the four kernels into degenerate kernels to separate the field and source point [13]. Later on, they applied the FMBEM to an oblique incident wave problem [14]. A FMBEM based on the Galerkin boundary integral was proposed by Fischer, Gauger and Gaul [15],

* Corresponding author. Tel.: +86 21 34206332x820; fax: +86 21 34205783.
E-mail address: wkjiang@sjtu.edu.cn (W. Jiang).

0955-7997/$ - see front matter © 2012 Elsevier Ltd. All rights reserved.
http://dx.doi.org/10.1016/j.enganabound.2012.09.011

which has a symmetric coefficient matrix but increases the time used in each iteration because of double integration on an element. The structure-acoustic coupling simulation by adopting FMBEM and FEM has been studied in the group leading by Fischer and Gaul [16–18]. Shen and Liu developed an adaptive FMBEM based on Burton–Miller formulation by extending the adaptive algorithm from 3D potential problems to 3D acoustic problems [19]. The adaptive FMBEM was then applied to solve half-space acoustic problems in conjunction with half-space Green' function and the RCR method [20], which can reduce CPU time and memory storage by half [21]. Later on, a new definition of interaction list was introduced by Bapat and Liu to reduce the M2L translation by about 30–40% and therefore can improve the efficiency of the FMBEM [22]. Tong and Chew employed the FMBEM to solve acoustic wave scattering problems by very large objects with 3D arbitrary geometries [23]. Solution of a model with 2 million unknowns on a workstation without involving parallel algorithms was reported therein. A LF FMBEM based on a variety of formulations has been presented by Yasuda et al. [24]. The LF FMBEM adopted a technique that uses the Taylor expansion for M2M and L2L translations, and the RCR with recurrence relations for M2L translation. A diagonal form FMBEM for 2D acoustic problems based on the Burton–Miller formulation was developed by Wu, Jiang and Liu [25]. Analytical moment expressions which are accurate and efficient in computation of moments on constant [26] and linear triangular [27] elements were developed by the authors. Recently, a FMBEM for 3D multi-domain acoustic scattering problems was developed in our group [28].

The FMBEMs introduced above have their preference frequency range and can be grouped into two types, named LF FMBEM and HF FMBEM (also referred as diagonal form FMBEM). Common views of the two types FMBEM are: LF FMBEM is stable in the low-frequency regime and requires less memory, while HF FMBEM is faster in the higher frequency but instable in the low-frequency, and needs more memory. In recent years, hybrid FMBEMs which are free of frequency division have been developed by Cheng et al. [29], Gumerov and Duraiswami [30]. The former switches to different representations at low and high frequencies, while the latter is based on a RCR scheme. From the practical point of view, some problems still remain for the LF FMBEM, especially when it is applied on higher frequency acoustic problems and no special treatment is taken. However, the numerical instability problems of the LF FMBEM are rarely mentioned except at the end of Ref. [30].

Burton–Miller [31] formulation is the widely used method in FMBEM to overcome the non-uniqueness problem at characteristic frequencies for exterior acoustic problems. The most difficult part in implementation of the Burton–Miller formation is the hypersingular integral. Lots of research has been devoted to alleviate the singularity. Chien et al. [32] employed some identities in the integral equation related to an interior Laplace problem to reduce the order of kernel singularity. A weakly singular form of the hypersingular integral by subtracting a two-term Taylor series from the density function are presented by Liu, Rizzo and Chen in Refs. [33,34]. Guiggiani et al. [35] proposed a general algorithm method to deal with hypersingular integrals which allows any hypersingular integral to be directly transformed into a sum of double and a one-dimensional regular integrals. A method based on multiple subtractions and additions to separate singular and regular integral terms in the polar transformation domain was developed by Karami and Derakhshan to evaluate the hypersingular integrals [36]. Methods to deal with hypersingular integral in Galerkin BEM are prosed in Refs [37,38]. Seydou et al. [39] proposed an approach to compute the singular and hypersingular parts of the integrals by a simple use of Green's theorem and particular solutions of the Helmholtz equations. Based on the method proposed by Chen et al. [40], an improved Burton–Miller was developed by Li and Huang [41]. Most of the methods introduced above are still cumbersome and require extremely complicated numerical procedure in general. Recently, explicit evaluation of hypersingular integrals for 3D acoustic problems discretized with constant triangular element were proposed by Matsmuto, Zheng et al. [42,43], and then was used in shape sensitivity analysis [44]. The resulting integrals for the element on which the field point lies consist of two regular line integrals of angular variables, as they said, those regular line integrals can be numerically evaluated by means of a standard Gaussian quadrature formula. We find that the two remaining regular line integrals of angular variables can be computed by an analytical method. This is another motivation of this paper.

This paper is organized as follows: The Burton–Miller formulations based on explicit hypersingular BIE for boundary discretization with constant triangular element are reviewed in Section 2. Analytical expression of the two regular line integrals left in the explicit hypersingular evaluation and its error analysis are described in Section 3. Section 4 consists of three parts, part one gives the definition of spherical function used in the LF FMBEM; in part two, formulations of translations are briefly reviewed, and reasons of numerical instability in translation are discussed; an algorithm of adopting the HF moment in the upward pass is developed in part three. Numerical examples are given in Section 5 to validate the explicit hypersingular integrals with analytical integration of the two remaining regular line integrals, and demonstrate the numerical instability of the LF FMBEM using RCR. The efficiency and accuracy of the improved LF FMBEM for higher frequency acoustic problems are also proved. Section 6 concludes the paper with some discussions.

2. Boundary integral formulation

The time harmonic acoustic waves in a homogeneous and isotropic acoustic medium E is described by the following Helmholtz equation:

$$\nabla^2\varphi(\mathbf{x})+k^2\varphi(\mathbf{x})=0, \quad \forall \mathbf{x}\in E, \tag{1}$$

where ∇^2 is the Laplace operator, $\varphi(\mathbf{x})$ is the sound pressure at point $\mathbf{x}$, k is the wavenumber defined by $k=\omega/c$, with ω being the angular frequency and c being the sound speed in medium E. By using the Green's second identity, the solution of Eq. (1) can be expressed by an integral representation:

$$\varphi(\mathbf{x})=\int_S\left[G(\mathbf{x},\mathbf{y})q(\mathbf{y})-\frac{\partial G(\mathbf{x},\mathbf{y})}{\partial \mathrm{n}(\mathbf{y})}\varphi(\mathbf{y})\right]dS(\mathbf{y})+\varphi^I(\mathbf{x}), \quad \forall \mathbf{x}\in E, \tag{2}$$

where $\mathbf{x}$ is a field point and $\mathbf{y}$ is a source point on boundary S, $q(\mathbf{y})$ is the normal gradient of sound pressure, defined as $q(\mathbf{y})=\partial\varphi(\mathbf{y})/\partial n(\mathbf{y})$ where the unit normal vector $n(\mathbf{y})$ on boundary S is defined to point outwards from E. Incident wave $\varphi^I(\mathbf{x})$ will not be presented for radiation problems. In this paper, the time convention adopted is using the factor $e^{-i\omega t}$, correspondingly, the free-space Green's function G for 3D problems is given by

$$G(\mathbf{x},\mathbf{y})=\frac{e^{ikr}}{4\pi r}, \text{ with } r=|\mathbf{x}-\mathbf{y}|. \tag{3}$$

To solve the integral Eq. (2), source point $\mathbf{x}$ should be moved to the boundary to generate the well-known conventional boundary integral equation (CBIE). The CBIE fails to give unique solutions for exterior acoustic problems at the fictitious frequencies of the associated interior problems. The Burton–Miller method [31] was proposed to overcome this non-uniqueness. It has been widely used in acoustic problems and been proved effective to circumvent the fictitious frequency problems. But it gives rise to a

hypersingular boundary integral equation (HBIE) which is the most difficult part in the implementation of the Burton–Miller method. Recently, an explicit evaluation of strongly singular and hypersingular boundary integral contained in the CBIE and HBIE for constant triangular element was proposed in Ref. [42].

Suppose the boundary is composed of constant triangular elements and the sound pressure $\varphi(\mathbf{x})$ satisfies $C^{1,\alpha}$ Hölder continuity, the CBIE and HBIE with explicit evaluation of strongly singular and hypersingular boundary integral are

$$\frac{1}{2}\varphi(\mathbf{x})+\int_{S\setminus\Delta_{\mathbf{x}}}\frac{\partial \mathrm{G}(\mathbf{x},\mathbf{y})}{\partial n(\mathbf{y})}\varphi(\mathbf{y})dS(\mathbf{y})=\int_{S\setminus\Delta_{\mathbf{x}}}G(\mathbf{x},\mathbf{y})q(\mathbf{y})dS(\mathbf{y}) +\frac{i}{2k}\left(1-\frac{1}{2\pi}\sum_{m=1}^{3}\int_{\theta_1^m}^{\theta_2^m}e^{ikR(\theta)}d\theta\right)q(\mathbf{x})+\varphi^I(\mathbf{x}), \tag{4}$$

$$\int_{S\setminus\Delta_{\mathbf{x}}}\frac{\partial^2 \mathrm{G}(\mathbf{x},\mathbf{y})}{\partial n(\mathbf{x})\partial n(\mathbf{y})}\varphi(\mathbf{y})dS(\mathbf{y})+\left(\frac{ik}{2}-\sum_{m=1}^{3}\int_{\theta_1^m}^{\theta_2^m}\frac{e^{ikR(\theta)}}{4\pi R(\theta)}d\theta\right)\varphi(\mathbf{x}) =\int_{S\setminus\Delta_{\mathbf{x}}}\left[\frac{\partial \mathrm{G}(\mathbf{x},\mathbf{y})}{\partial n(\mathbf{x})}q(\mathbf{y})\right]dS(\mathbf{y})-\frac{1}{2}q(\mathbf{x})+q^I(\mathbf{x}), \tag{5}$$

where $S\setminus\Delta_{\mathbf{x}}$ denotes the boundary S excluding the boundary element on which the field point $\mathbf{x}$ is located, angles θ_1^m and θ_2^m are demonstrated in Fig. 1. In the next section, we will give an analytical expression of the two regular line integrals appearing in Eqs. (4) and (5) on the element where the field point is located.

A linear combination of Eqs. (4) and (5) with a properly selected complex coupling constant β, such as $\beta=i/k$, yields the Burton–Miller formulation for constant triangular element:

$$\frac{1}{2}\varphi(\mathbf{x})+\mathcal{D}\varphi(\mathbf{y})+\beta\mathcal{H}\varphi(\mathbf{y})+\beta\dot{\mathcal{R}}_{\Delta_{\mathbf{x}}}\varphi(\mathbf{x}) =\mathcal{S}q(\mathbf{y})+\beta\mathcal{M}q(\mathbf{y})+\mathcal{R}_{\Delta_{\mathbf{x}}}q(\mathbf{x})-\frac{\beta}{2}q(\mathbf{x})+\varphi^I(\mathbf{x})+\beta q^I(\mathbf{x}), \tag{6}$$

in which

$$\mathcal{S}q(\mathbf{y})=\int_{S\setminus\Delta_{\mathbf{x}}}G(\mathbf{x},\mathbf{y})q(\mathbf{y})dS(\mathbf{y}), \tag{7}$$

$$\mathcal{D}\varphi(\mathbf{y})=\int_{S\setminus\Delta_{\mathbf{x}}}\frac{\partial \mathrm{G}(\mathbf{x},\mathbf{y})}{\partial n(\mathbf{y})}\varphi(\mathbf{y})dS(\mathbf{y}), \tag{8}$$

$$\mathcal{M}q(\mathbf{y})=\int_{S\setminus\Delta_{\mathbf{x}}}\frac{\partial \mathrm{G}(\mathbf{x},\mathbf{y})}{\partial n(\mathbf{x})}q(\mathbf{y})dS(\mathbf{y}), \tag{9}$$

$$\mathcal{H}\varphi(\mathbf{y})=\int_{S\setminus\Delta_{\mathbf{x}}}\frac{\partial^2 \mathrm{G}(\mathbf{x},\mathbf{y})}{\partial n(\mathbf{x})\partial n(\mathbf{y})}\varphi(\mathbf{y})dS(\mathbf{y}), \tag{10}$$

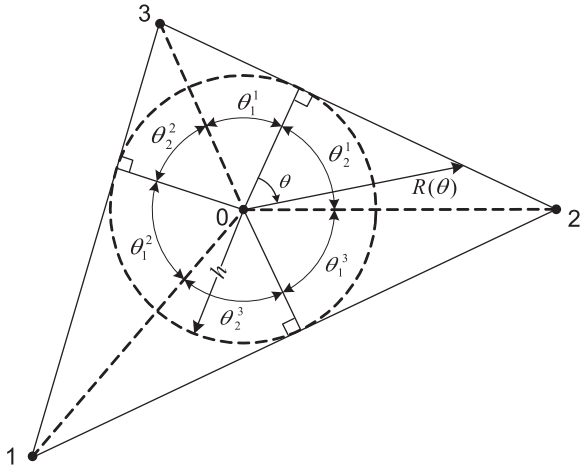

Fig. 1. Integral on an element.

$$\mathcal{R}_{\Delta_{\mathbf{x}}}=\frac{ik}{2}-\frac{1}{4\pi}\sum_{m=1}^{3}\int_{\theta_1^m}^{\theta_2^m}\frac{e^{ikR(\theta)}}{R(\theta)}d\theta, \tag{11}$$

$$\dot{\mathcal{R}}_{\Delta_{\mathbf{x}}}=\frac{i}{2k}\left(1-\frac{1}{2\pi}\sum_{m=1}^{3}\int_{\theta_1^m}^{\theta_2^m}e^{ikR(\theta)}d\theta\right). \tag{12}$$

Eq. (6) can give unique solutions at all frequencies for exterior acoustic problems, and its solution is accelerated by the fast multipole method.

3. Analytical expression of the regular line integrals on the triangular element

3.1. Formulations

Numeral integration methods are available to compute the two regular line integrals appearing in Eqs. (4) and (5). But, in this section, those integrals are described in detail to get analytical expression which is accurate and easier to control the error. As shown in Fig. 1, the triangle composes of three vertexes, denoted as 1, 2 and 3. The geometry center of the triangle is denoted as 0. Lines connecting the geometry center and other three vertexes divide the triangle into three smaller triangles where the regular line integrals are carried out. To calculate the line integral on those smaller triangles, the perpendicular line from the center to one side of the triangular element is treated as the polar axis which further divides the smaller triangles into two smaller triangles. According to the above configuration of coordinates, there are actually six smaller triangles in which the two regular line integrals need to be carried out for an element. If the geometry is chosen to be the center of inscribed circle of the triangle, as we used in Fig. 1, integrals only need to be computed on three smaller triangles due to the symmetry. One of the smaller triangles, as shown in Fig. 2, is taken as an example to derive the analytical expression.

Denote the corresponding two regular line integrals as

$$I_1=\int_0^{\theta_2^1}e^{ikR(\theta)}d\theta, \tag{13}$$

$$I_2=\int_0^{\theta_2^1}\frac{e^{ikR(\theta)}}{R(\theta)}d\theta \tag{14}$$

in which $R(\theta)=h/\cos\theta$. Appling the power series expansion of exponent function and exchanging the integral and summation order in Eqs. (13) and (14) yield

$$I_1=\sum_{n=0}^{\infty}\frac{(ikh)^n}{n!}\int_0^{\theta_2^1}\sec^n\theta\,d\theta, \tag{15}$$

$$I_2=\frac{\sin\theta_2^1}{h}+ik\sum_{n=0}^{\infty}\frac{(ikh)^n}{(n+1)!}\int_0^{\theta_2^1}\sec^n\theta\,d\theta \tag{16}$$

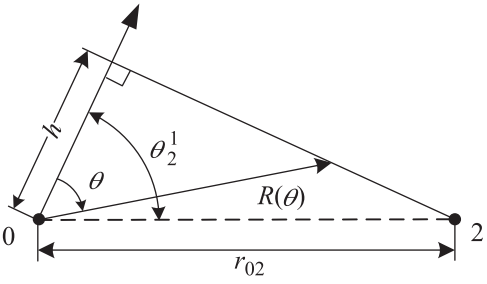

Fig. 2. Integral on a smaller triangle.

in which $\sec\theta = 1/\cos\theta$. Therefore, the computation of I_1 and I_2 relies on the integration of powers of secant function. We divide the integration of powers of secant function into two cases: n is even and n is odd. For the even $n=2m$, $m=0,1,\ldots$, the integration of even power of secant function can be written as

$$\int_0^{\theta_2^1} \sec^{2m}\theta\, d\theta = \begin{cases} \sum_{l=0}^{m-1} \frac{1}{2l+1}\binom{m-1}{l}\left(\tan\theta_2^1\right)^{2l+1}, & for\ m\neq 0 \\ \theta_2^1, & for\ m=0 \end{cases}, \tag{17}$$

in which binomial identity is used and $\binom{*}{*}$ is the binomial coefficient. For odd n, using the secant reduction formula, the integration of odd power of secant function has the following recursive relation

$$\int_0^{\theta_2^1} \sec^n\theta\, d\theta = \frac{\sec^{n-1}\theta_2^1 \sin\theta_2^1}{n-1} + \frac{n-2}{n-1}\int_0^{\theta_2^1} \sec^{n-2}\theta d\theta, \text{ for n} \neq 1, \tag{18}$$

in which the initial value is

$$\int_0^{\theta_2^1} \sec\theta\, d\theta = log\left(\sec\theta_2^1 + \tan\theta_2^1\right). \tag{19}$$

Combing Eqs. (17)–(19), the integration of powers of secant function can be evaluated exactly. Once the integration of powers of secant function is done, I_1 and I_2 can be computed with different coefficients as indicated in Eqs. (15) and (16).

In the evaluation of I_1 and I_2, series expansions are truncated. The selected truncation number is very crucial to the accuracy of those integrals. Since the integration of powers of secant function can be computed exactly, errors come from series expansion of the exponent function. Obviously, series expansions of kernels $e^{ikR(\theta)}$ and $e^{ikR(\theta)}/R(\theta)$ with $N-1$ truncated number share the same relative error which can be expressed as:

$$\left|\sum_{n=N}^{\infty} \frac{(ikR(\theta))^n}{n!}\right| \leq \sum_{n=N}^{\infty} \frac{(kR(\theta)_{max})^n}{n!} \leq \varepsilon, \tag{20}$$

in which ε is the desired relative error, and $R(\theta)_{max}=r_{02}$ as indicated in Fig. 2. As shown in Eq. (20), N is determined by the size of $kR(\theta)_{max}$. To derive a general method of N selection, we resort to the engineering empirical rule in the mesh generation, that is, for *every wavelength* (λ) *one should have at least six elements*. We roughly assume that $r_{02} \leq \lambda/7$ since r_{02} is smaller than the element size. In that sense, $kR(\theta)_{max} \leq 2\pi/7 = 0.898$ can be guaranteed especially when using the fast multipole boundary element method where the number of elements is generally larger than the above number determined by the engineering empirical rule. Therefore, with $\gamma = kR(\theta)_{max} \leq 1$, the following formula can be used to check whether N is large enough for the given ε:

$$\sum_{n=N}^{\infty} \frac{(kR(\theta)_{max})^n}{n!} \leq \frac{\gamma^N}{1-\gamma}\frac{1}{N!} \leq \varepsilon. \tag{21}$$

To describe quantitatively the relation of N with $kR(\theta)_{max}$. The error bounds of different truncation numbers and several γ are listed in Table 1by computing with

$$\xi = \sum_{n=N}^{\infty} \frac{(kR(\theta)_{max})^n}{n!}. \tag{22}$$

Even though Eq. (20) just gives the relative errors of series expansion of the exponent function, actually it can also be used to describe the relative errors of the computation of I_1 and I_2. Take I_2 as an example for which the relative error can be expressed as:

$$\varepsilon(I_2) = \left|\frac{\int_0^{\theta_2^1} \frac{1}{R(\theta)}\sum_{n=N}^{\infty}\frac{(ikR(\theta))^n}{n!}d\theta}{\int_0^{\theta_2^1}\frac{e^{ikR(\theta)}}{R(\theta)}d\theta}\right| \leq \frac{R\left(\tilde{\theta}\right)}{h}\xi < \frac{r_{02}}{h}\xi, \tag{23}$$

in which the mean value theorem of integral is used and $\tilde{\theta}$ is a point in the range $\left(0,\theta_1^2\right)$. If the triangle element is regularly configured, the relative error of I_2 computation can be viewed at the same level of that in the exponent function computation with series expansion. It is worth noting that the relative error of I_1 computation is the same as that of the exponent function computation with series expansion since the denominator $R(\theta)$ in Eq. (23) is equal to one.

Table 1
The error bound computed with Eq. (22) for different N and γ.

N	$\gamma = kR(\theta)_{max}$				
	0.898	0.5	0.25	0.1	0.09
4	5.16E-02	3.28E-02	2.89E-03	1.71E-04	4.25E-06
5	9.95E-03	5.70E-03	2.84E-04	8.49E-06	8.47E-08
6	1.62E-03	8.33E-04	2.34E-05	3.52E-07	1.41E-09
7	2.26E-04	1.05E-04	1.65E-06	1.25E-08	2.01E-11
8	2.79E-05	1.16E-05	1.03E-07	3.89E-10	2.51E-13
9	3.06E-06	1.15E-06	5.66E-09	1.08E-11	2.78E-15
10	3.03E-07	1.02E-07	2.82E-10	2.69E-13	2.78E-17
11	2.73E-08	8.29E-09	1.28E-11	6.10E-15	2.53E-19
12	2.26E-09	6.16E-10	5.30E-13	1.27E-16	2.10E-21

3.2. Numerical validation

From above analysis we know that the two remaining regular line integrals can be evaluated as accurate as possible in the sense of machine precision. To prove benefits of the method developed above, the accuracy and efficiency of weakly singular and hypersingular integrals are compared with those computed by the Gaussian quadrature method, and the singular subtraction method [33] for different cases. The formulations of singular subtraction of weakly singular and hypersingular integrals for constant element are

$$\int_{\Delta_{\mathbf{x}}} G(\mathbf{x},\mathbf{y})dS(\mathbf{y}) = \int_{\Delta_{\mathbf{x}}} [G(\mathbf{x},\mathbf{y}) - \overline{G}(\mathbf{x},\mathbf{y})]dS(\mathbf{y}) + \int_{\Delta_{\mathbf{x}}} \overline{G}(\mathbf{x},\mathbf{y})dS(\mathbf{y}), \tag{24}$$

$$\int_{\Delta_{\mathbf{x}}} \frac{\partial^2 G(\mathbf{x},\mathbf{y})}{\partial n(\mathbf{x})\partial n(\mathbf{y})}dS(\mathbf{y}) = \int_{\Delta_{\mathbf{x}}} \frac{\partial^2 [G(\mathbf{x},\mathbf{y}) - \overline{G}(\mathbf{x},\mathbf{y})]}{\partial n(\mathbf{x})\partial n(\mathbf{y})}dS(\mathbf{y}) + \int_{\Delta_{\mathbf{x}}} \frac{\partial^2 \overline{G}(\mathbf{x},\mathbf{y})}{\partial n(\mathbf{x})\partial n(\mathbf{y})}dS(\mathbf{y}), \tag{25}$$

in which $\overline{G}(\mathbf{x},\mathbf{y}) = 1/4\pi r$ is the static fundamental solution, and the added back terms can be evaluated with analytical formulas. The first integral is evaluated using Gaussian quadrature since it is only weakly singular after the subtraction. Two kinds of triangular elements are set up for the test, one is named regular (equilateral triangle) and another is irregular (isosceles triangle). The quality of the triangular element is described by the aspect ratio defined by the ratio of the longest side length over the minimal height of the triangle. Therefore the aspect ratio of the regular element is $\sqrt{3}/2$, which is the best aspect ratio of a triangle. The irregular element is configured to have an aspect ratio of 40.

Two wavenumbers are selected to let $kR(\theta)_{max}=0.1$ and 0.898, respectively. The relative errors of different cases are listed in

Table 2
Relative errors of singular integrals by different method of $kR(\theta)_{max}=0.1$.

Methods	Term or point	Relative error			
		Regular element		Irregular element	
		Weaksingular	Hypersingular	Weaksingular	Hypersingular
Explicit analytical	4	0.345609E-11	0.183505E-07	0.748418E-14	0.508850E-08
	6	0.155103E-15	0.840761E-12	0.000000E+00	0.264864E-12
	8	0.000000E+00	0.000000E+00	0.000000E+00	0.000000E+00
Explicit Gaussian	6	0.947767E-10	0.168353E-06	0.195126E-06	0.443423E-01
	12	0.620491E-15	0.241297E-13	0.101683E-07	0.231200E-02
	64	0.466219E-15	0.226956E-13	0.272154E-15	0.249241E-12
Singular subtraction	6	0.386950E-03	0.195125E-04	0.471373E-05	0.610273E-05
	12	0.179098E-03	0.179257E-05	0.133865E-02	0.321967E-06
	64	0.768859E-04	0.110399E-06	0.833647E-06	0.187908E-07

Table 3
Relative errors of singular integrals by different method of $kR(\theta)_{max}=0.898$.

Methods	Term or point	Relative error			
		Regular element		Irregular slement	
		Weaksingular	Hypersingular	Weaksingular	Hypersingular
Explicit analytical	4	0.189457E-05	0.119751E-03	0.391041E-08	0.331374E-04
	6	0.525100E-08	0.442612E-06	0.123166E-10	0.139192E-06
	8	0.101707E-10	0.107172E-08	0.272474E-13	0.383632E-09
Explicit Gaussian	6	0.894203E-08	0.231859E-06	0.157515E-04	0.449388E-01
	12	0.189493E-14	0.544280E-13	0.835234E-06	0.248167E-02
	64	0.708789E-15	0.172698E-14	0.680723E-15	0.316041E-13
Singular subtraction	6	0.326970E-01	0.160220E-02	0.380337E-03	0.499535E-03
	12	0.151197E-01	0.145537E-03	0.107987E+00	0.262450E-04
	64	0.648959E-02	0.894902E-05	0.672488E-04	0.152443E-05

Tables 2 and 3. The relative error is defined as

$$\text{Relative error} = \frac{|numerical - analytical|}{|analytical|}, \tag{26}$$

in which *numerical* means singular integrals computed by the explicit analytical method (developed above), the explicit Gaussian quadrature (explicit singular integrals with Gaussian quadrature evaluation) and the singular subtraction method. Analytical results of singular integrals are computed by the analytical expression with large enough truncation number to let evaluation of the integral reach the machine precision. *Term* or *Point* in Tables 2 and 3 means truncation number for explicit analytical method and number of Gaussian quadrature point for Explicit Gaussian and Singular subtraction methods.

Careful observation in Tables 2 and 3 can make a conclusion that the larger the element size (in the sense of wavelength) is, the more term or point is needed for the three methods. For the explicit Gaussian method, results on the irregular element are worse than the regular element. But the explicit analytical method does not produce the same phenomena because the bounded error of the irregular element is worse than that of the regular element cannot guarantee the real relative error follows the same relation as that of bounded errors. If the Gaussian point does not locate at the singular points, the singular subtraction can give a good accuracy, otherwise the result is worse. Whatever, results of the explicit Gaussian method and the singular subtraction method largely depend on the size and shape of the element. In contrast, the explicit analytical method of the singular integrals is flexible because its error just relates to $kR(\theta)_{max}$ and is less sensitive to the element shape limitation than the other two methods. The CPU time to compute the two singular integrals for different terms and nodes are summarized in Table 4. Clearly, the explicit analytical method is more efficient than the other two methods.

Table 4
CPU time of singular integrals for the three methods with different term or point.

Methods	Term or point	CPU time
Explicit analytical	4	0.104535E-05
	6	0.141965E-05
	8	0.193484E-05
Explicit Gaussian	6	0.173969E-04
	12	0.347245E-04
	64	0.441819E-03
Singular subtraction	6	0.196537E-05
	12	0.297956E-05
	64	0.116582E-04

4. Formulations of FMBEM

Discretizing the boundary S using N constant triangular elements leads Eq. (6) to a N dimensional linear equations' systems whose solving can be accelerated by the fast multipole method with a iterative solver, such as GMRES. In this section, the multiple expansion and translation formulations are briefly reviewed. Reasons of numerical instability in translation are discussed. An algorithm to improve the efficiency of the computation of moments is presented.

4.1. Multipole expansion

The free-space Green's function can be expressed by multipole expansion. Please note that the normalized associate Legendre

functions and special harmonic functions used in this paper are different from that in our previous papers [19,21,22], which are in the form

$$\overline{\mathrm{P}_n^m}(x)=(-1)^m\sqrt{\frac{2n+1}{2}\frac{(n-|m|)!}{(n+|m|)!}}\mathrm{P}_n^{|m|}(x),\quad -1\le x\le 1, \tag{27}$$

$$Y_n^m(\theta,\phi)=\frac{1}{\sqrt{2\pi}}\overline{\mathrm{P}_n^m}(\cos\theta)e^{im\varphi},\quad 0\le\theta\le\pi,\ 0\le\phi\le 2\pi. \tag{28}$$

Therefore the multipole expansion of Green's function near point $\mathbf{y}_c$ is

$$G(\mathbf{x},\mathbf{y})=ik\sum_{n=0}^{\infty}\sum_{m=-n}^{n}O_n^m(k,\mathbf{x},\mathbf{y}_c)I_n^{-m}(k,\mathbf{y},\mathbf{y}_c),\ |\mathbf{y}-\mathbf{y}_c|<|\mathbf{x}-\mathbf{y}_c|, \tag{29}$$

where the inner function is defined by

$$I_n^m(k,\mathbf{x},\mathbf{y}_c)=j_n(k|\mathbf{y}-\mathbf{y}_c|)\mathrm{Y}_n^m\left(\frac{\mathbf{y}-\mathbf{y}_c}{|\mathbf{y}-\mathbf{y}_c|}\right), \tag{30}$$

and the outer function is defined by

$$O_n^m(k,\mathbf{x},\mathbf{y}_c)=h_n(k|\mathbf{x}-\mathbf{y}_c|)\mathrm{Y}_n^m\left(\frac{\mathbf{x}-\mathbf{y}_c}{|\mathbf{x}-\mathbf{y}_c|}\right) \tag{31}$$

In Eqs. (30) and (31), j_n is the nth order spherical Bessel function of the first kind; h_n is the nth order spherical Hankel function of the first kind.

For a source element Δ_j which is far from the field element where the field point $\mathbf{x}$ is located, Eq. (29) can be used to translate the contribution from an element Δ_j to a contribution collecting center $\mathbf{y}_c$. The collected contributions from specific elements are named multipole moment. The multipole moment for operators $\mathcal{S}$ and $\mathscr{M}$ is in the form

$$\mathrm{M}_n^m(k,\mathbf{y}_c)=\int_{\Delta_j}I_n^m(k,\mathbf{x},\mathbf{y}_c)q(\mathbf{y})dS(\mathbf{y}), \tag{32}$$

and the multipole moment for operators $\mathcal{D}$ and $\mathscr{H}$ is in the form

$$\mathrm{M}_n^m(k,\mathbf{y}_c)=\int_{\Delta_j}\frac{\partial}{\partial n(\mathbf{y})}I_n^m(k,\mathbf{x},\mathbf{y}_c)\varphi(\mathbf{y})dS(\mathbf{y}). \tag{33}$$

4.2. Formulations of translations

In the fast multipole BEM, once the moments are computed, the final evaluation of the contribution from far away source elements to the field elements generally consists of three types of translation, moment to moment (M2M), moment to local (M2L) and local to local (L2L), between levels and cells.

If the center $\mathbf{y}_c$ is moved to another position $\mathbf{y}_{c'}$, the moments can be translated by the following M2M method

$$\mathrm{M}_{n'}^{m'}(k,\mathbf{y}_{c'})=\sum_{n=0}^{\mathrm{P}}\sum_{m=-n}^{n}(\mathrm{M}|\mathrm{M})_{n,n'}^{m,m'}(k,\mathbf{t})\mathrm{M}_n^m(k,\mathbf{y}_c),\ \text{for } 0\le|m'|\le n'\le\mathrm{P}', \tag{34}$$

for $|\mathbf{y}-\mathbf{y}_{c'}|<|\mathbf{x}-\mathbf{y}_{c'}|$, in which we assume P' and P are orders of the moment associated with center $\mathbf{y}_{c'}$ and $\mathbf{y}_c$ correspondingly, $\mathbf{t}=\mathbf{y}_c-\mathbf{y}_{c'}$. An approach to compute the M2M translation coefficients is

$$(\mathrm{M}|\mathrm{M})_{n,n'}^{m,m'}(k,\mathbf{t})=\sum_{l=0}^{(n+n'-|n-n'|)/2}W_{|n-n'|+2l,n',n}^{m'-m,m',m}I_{|n-n'|+2l}^{m-m'}(k,\mathbf{t}), \tag{35}$$

in which W is purely numerical and can be computed by

$$W_{n'',n',n}^{m'',m',m}=4\pi m''\varepsilon_{-m'}\varepsilon_m i^{n''+n'-n}\left[\frac{(2n''+1)(2n'+1)(2n+1)}{4\pi}\right]^{\frac{1}{2}}\begin{pmatrix}n'' & n' & n\\ 0 & 0 & 0\end{pmatrix}\begin{pmatrix}n'' & n' & n\\ m'' & -m' & m\end{pmatrix}, \tag{36}$$

where $\begin{pmatrix}* & * & *\\ * & * & *\end{pmatrix}$ denotes the wigner-3j symbol,

$$\varepsilon_m=\begin{cases}(-1)^m, & m>0\\ 1, & m\le 0\end{cases}$$

The L2L formulation is the same as Eq. (34) but with moments replaced with local expansion coefficients:

$$\mathrm{L}_{n'}^{m'}(k,\mathbf{x}_{c'})=\sum_{n=0}^{\mathrm{P}}\sum_{m=-n}^{n}(\mathrm{L}|\mathrm{L})_{n,n'}^{m,m'}(k,\mathbf{t})\mathrm{L}_n^m(k,\mathbf{x}_c),\ \text{for } 0\le|m'|\le n'\le\mathrm{P}' \tag{37}$$

in which $\mathbf{t}=\mathbf{x}_c-\mathbf{x}_{c'}$. The L2L is the reverse process of M2M. It shares the same translation coefficients expression, Eq. (35).

The local expansion coefficient of a cell whose center is $\boldsymbol{x}_c$ is realized by collecting moments in its interaction list:

$$\mathrm{L}_{n'}^{m'}(k,\mathbf{x}_c)=\sum_{n=0}^{\mathrm{P}}\sum_{m=-n}^{n}(\mathrm{M}|\mathrm{L})_{n,n'}^{m,m'}(k,\mathbf{t})\mathrm{M}_n^m(k,\mathbf{y}_c),\ \text{for } 0\le|m'|\le n'\le\mathrm{P}', \tag{38}$$

for $|\mathbf{x}-\mathbf{x}_c|<|\mathbf{y}-\mathbf{x}_c|$ and $|\mathbf{y}-\boldsymbol{y}_c|<|\mathbf{x}-\mathbf{y}_c|$, in which $\boldsymbol{t}=\mathbf{y}_c-\mathbf{x}_c$, the translation coefficients are

$$(\mathrm{M}|\mathrm{L})_{n,n'}^{m,m'}(k,\mathbf{t})=\sum_{l=0}^{(n+n'-|n-n'|)/2}W_{|n-n'|+2l,n',n}^{m'-m,m',m}O_{|n-n'|+2l}^{m-m'}(k,\mathbf{t}). \tag{39}$$

The fast multipole formulation discussed above is an $O(p^5)$ algorithm which is rarely used in FMBEM except for the simulation of very low-frequency acoustic problems. For complete analysis, its formulations are provided here. Actually one widely used formulation for low-frequency problems is the $O(p^3)$ algorithm developed by Gumerov and Duraiswami [20,45]. They proposed a rotation-coaxial-rotation back (RCR) decomposing of the M2M, M2L and L2L translation which results in $O(p^3)$ complexity because rotation and coaxial process are all $O(p^3)$. Translations of moments and local expansion coefficients can be computed by the following decomposing

$$(\mathbf{F}|\mathbf{E})(\mathrm{k},\mathbf{t})\mathbf{C}=\mathbf{Rot}\left(Q^{-1}\right)(\mathbf{F}|\mathbf{E})_{\mathrm{coax}}(\mathrm{k},\mathbf{t})\mathbf{Rot}(Q)\mathbf{C}, \tag{40}$$

where $\boldsymbol{Rot}(Q)$ is the rotation matrix, $(\boldsymbol{F}|\boldsymbol{E})_{\mathrm{coax}}(\mathrm{k},\ \boldsymbol{t})$ is the coaxial translation matrix, $\boldsymbol{C}$ is a rotating vector composing of moments or local expansion coefficients, both operators $\boldsymbol{E}$ and $\boldsymbol{F}$ represent either moments (M) or local expansion operator (L).

The rotation translation is designed to rotate the coordinates to a new coordinates where the oriented translation vector is along the positive z-axis. The rotation in essence is to rotate the spherical harmonic of a specific degree, and is a well-studied problem arising in classical scattering theory, quantum mechanics and numerical analysis. Recurrence method is a widely used approach to compute the entries of the rotation matrix [20,46,47]. It is fast but subject to a variety of instabilities which limits the effectiveness of rotation computation for high degree. A recursive back propagation method introduced by Gumerov (p336, in Ref. [48]), and a fast and stable method using "pseudospectral" projection proposed by Gimbutas and Greengard [49] are available to compute rotation accurately. Therefore numerical instability of rotation computation in RCR is not an issue anymore, but users should choose a proper method according to their problems.

By exploring the fact that in the coaxial translation the spherical polar angle ϕ is not changed, and due to the

orthogonality of the functions $e^{im\phi}$, stating that they can be expanded over the basis function of same order m only, the coaxial translation is thus can be expressed by

$$\mathrm{E}_{n'}^{\tilde{m}} = \sum_{n=|m|}^{\mathrm{P}} (\mathrm{F}|\mathrm{E})_{n,n'}^{\tilde{m}} \mathrm{F}_{n}^{\tilde{m}}, \text{ for } |\tilde{m}| \le n' \le \mathrm{P}', \ |\tilde{m}| \le n \le P, \tag{41}$$

where $|\tilde{m}| \le min(\mathrm{P}',\mathrm{P})$, E represents either moments or local expansions, while F just represents moments. Another explanation of Eq. (41) comes from the fact that $\theta_{\mathbf{t}}=0$, $\overline{\mathrm{P}_n^m}(\cos\theta_{\mathbf{t}})=0$ for $m\neq 0$, and in light of Eqs. (35) and (39), the translation coefficients $(\mathrm{F}|\mathrm{E})_{n,n'}^{m,m'}=0$ for $m\neq m'$. It is worth noting that generally in the M2M translation $\mathrm{P}'\ge\mathrm{P}$, obviously the translated coefficients $\mathrm{E}_{n'}^{m'}=0$ for $\mathrm{P}<|m'|\le\mathrm{P}'$ after the coaxial translation. Actually, it is not true for the real coefficients centering at where $\mathrm{E}_{n'}^{m'}$ is located. But after rotation back, those coefficients are generally non-zero and very small. It will not introduce serious errors to the final results on the condition that the selected multipole expansion order at each level satisfying the prescribed tolerance.

4.3. Using the diagonal form moment in the upward pass

The plane wave

$$e^{-ik(\mathbf{y}-\mathbf{y}_c)\cdot\hat{\boldsymbol{\sigma}}} = 4\pi \sum_{n=0}^{\mathrm{P}} \sum_{m=-n}^{n} (-i)^n I_n^m(k,\mathbf{y},\mathbf{y}_c) Y_n^{-m}(\hat{\boldsymbol{\sigma}}) + \varepsilon, \tag{42}$$

in which $\hat{\boldsymbol{\sigma}}$ is a point on a unit sphere, $|\varepsilon|$ is the relative error of the above series expansion with the first P terms:

$$\varepsilon = \sum_{n=\mathrm{P}+1}^{\infty} (-i)^n (2n+1) j_n(k|\mathbf{y}-\mathbf{y}_c|) P_n\left(\hat{\boldsymbol{\sigma}}\cdot\frac{\mathbf{y}-\mathbf{y}_c}{|\mathbf{y}-\mathbf{y}_c|}\right), \tag{43}$$

The partial wave expansion of the plane wave and addition theorem of Legendre function, P_n, are used in Eqs. (42) and (43). Therefore the multipole moment for operators $\mathcal{S}$ and $\mathscr{M}$ can also be expressed as

$$M_n^m(k,\mathbf{y},\mathbf{y}_c) = \frac{i^n}{4\pi}\int_{\sigma_1} Y_n^m(\hat{\boldsymbol{\sigma}}) M_{HF}(\hat{\boldsymbol{\sigma}},\mathbf{y},\mathbf{y}_c) d\sigma + \int_{\sigma_1} \varepsilon Y_n^m(\hat{\boldsymbol{\sigma}}) d\sigma, \tag{44}$$

in which $M_{HF}(\hat{\boldsymbol{\sigma}},\mathbf{y},\mathbf{y}_c)$ is the corresponding moment in the diagonal form FMBEM, named the high-frequency moment:

$$M_{HF}(\hat{\boldsymbol{\sigma}},\mathbf{y},\mathbf{y}_c) = \int_{\Delta_j} e^{-ik(\mathbf{y}-\mathbf{y}_c)\cdot\hat{\boldsymbol{\sigma}}} q(\mathbf{y}) dS(\mathbf{y}). \tag{45}$$

For operators $\mathcal{D}$ and $\mathscr{H}$, the translation is same to Eq. (44) but with the diagonal form moment as:

$$M_{HF}(\hat{\boldsymbol{\sigma}},\mathbf{y},\mathbf{y}_c) = -\int_{\Delta_j} \left(\frac{\partial\mathbf{y}}{\partial n(\mathbf{y})}\cdot\hat{\boldsymbol{\sigma}}\right) e^{-ik(\mathbf{y}-\mathbf{y}_c)\cdot\hat{\boldsymbol{\sigma}}} q(\mathbf{y}) dS(\mathbf{y}). \tag{46}$$

It is worth noting that similar to the analysis in Eq. (23), the relative error of the translation from the high-frequency moment to the low-frequency moment can be viewed at the same level of $|\varepsilon|$.

Therefore, if P is selected properly to let $|\varepsilon|$ be less than a given tolerance, the accuracy of the translation in Eq. (44) can be guaranteed. The integral over the unit sphere in the translation is computed exactly with $P+1$ Gaussian quadrature in the θ direction and $2P+1$ trapezodial rule in the ϕ direction. Since ϕ is equally spaced, the translation can also be accelerated by the FFT which results in an $O(2\mathrm{P}^3)$ complexity.

Advantages are manifested for adopting the diagonal form moments in the upward pass of the low-frequency FMBEM for higher frequency acoustic problems analysis. It is faster to use the diagonal moments than to use the RCR method in the upward pass. Because analytical integration [26] is available for the moment computation, and the overall complexity of M2M using the diagonal form moment and then translate it to the low-frequency moment is $O(2\mathrm{P}^3)$. In contrast, the complexity of M2M using RCR is $O(3\mathrm{P}^3)$. The efficiency of the improved LF FMBEM is validated in the numerical examples. Even though the LF FMBEM is not efficient and has drawbacks in the M2M translation, its memory requirement for storing the moments is low. That is one of reasons why we translate the diagonal form moment to the low-frequency format for later translations.

5. Numerical examples

In this section, numerical examples are presented to demonstrate the accuracy of the analytical hypersingular integral first, and then the efficiency and accuracy of the LF FMBEM for higher frequency acoustic problems analysis with the diagonal form moment in the upward pass are proved. In the following examples, the LF FMBEM based on RCR in both upward and downward passes is termed as A1. The LF FMBEM using diagonal moments in the upward pass and RCR in the downward pass is termed as A2. The diagonal FMBEM developed in the Ref [26] is termed as A3 in this paper. All three FMBEMs are implemented with the explicit singular BIEs method using the analytical approach to compute the remaining regular line integrals.

The GMRES solver is used and the tolerance is set at 10^{-4}. Left precondition based on the leaf cell is used in the iteration to accelerate the convergence ratio. The multipole expansion order is given by the empirical formula [50] as

$$\mathrm{p} = kd + c_0 log(kd+\pi) \tag{47}$$

where d is the diameter of the cell on which integration are calculated, and c_0 is a number to determine the desired accuracy, which is set to 5 in simulations. All simulations are done on a desktop PC with a 64-bit Intel® CoreTM2 Duo CPU and 8GB RAM, but only one core is used in the computation.

5.1. Interior problem of a pulsating sphere

A pulsating sphere with given constant boundary conditions is chosen as an interior example to verify accuracy of the FMBEM based on the analytical singular BIEs. The radius of the sphere is $a=0.5$ m, and its surface vibrates with normal velocity $v_n=0.1$ m/s which relates to the boundary condition by $\partial\varphi/\partial n = i\rho\omega v$. The mass density of acoustic medium is $\rho=1.2$ kg/m^3. Analytical boundary solution is given by

$$\varphi(a) = \frac{i\rho\omega v_n a}{ika-1} \tag{48}$$

In this case, the nondimensional value ka increases from 0.05 to 2.5, N is set to 4 in both Eq. (15) and Eq. (16). The L2 relative error of boundary solution is defined as

$$\epsilon_\varphi = \frac{\|\varphi_{FMBEM}-\varphi_{ana}\|}{\|\varphi_{ana}\|} \tag{49}$$

in which sound pressure φ_{FMBEM} is solved by the FMBEM, and φ_{ana} is computed by Eq. (48).

In Table 5, γ is the same as the one in Table 1, "—" means the solution is not correct due to the numerical instability of A3 for low-frequency problems analysis. This example validates the analytical singular BIEs, demonstrates the accuracy of the analytical formulations for the two remaining regular line integrals on the field element. Conclusion can also be made from Table 5 that the solution efficiency of the three algorithms is ranked from high to low as A3, A2 and A1. The reason is obvious because the overall complexity of

Table 5
Results of interior radiation of a pulsating sphere.

ka	DOFs	γ	ϵ_φ			CPU time		
			A1	A2	A3	A1	A2	A3
0.05	432	1.22E-2	6.20E-3	6.20E-3	—	3.12E-1	2.65E-1	–
0.5	768	9.33E-2	3.73E-3	3.73E-3	3.84E-3	4.99E-1	2.03E-1	1.09E-1
1.0	1,200	1.51E-1	2.68E-3	2.68E-3	2.70E-3	9.67E-1	5.15E-1	2.81E-1
1.5	2,352	1.63E-1	1.59E-3	1.56E-3	1.58E-3	2.37E+0	1.48E+0	5.15E-1
2.0	4,332	1.61E-1	1.71E-3	9.86E-4	1.01E-3	3.82E+0	2.26E+0	1.28E+0
2.5	7,500	1.53E-1	8.34E-4	1.02E-3	7.32E-4	8.02E+0	5.21E+0	1.76E+0

A3 is $O(P^2 logP)$, the upward pass in A2 is $O(P^2 logP)$ while the down pass is $O(P^3)$, and the overall complexity of A1 is $O(P^3)$.

5.2. Scattering from a rigid sphere

In this example, a rigid sphere impinged by a plane wave traveling along $+z$ direction with unit amplitude is investigated to verify the Burton–Miller formulation based on the analytical singular BIEs. The nondimensional value ka (a is also the radius) ranges from 2.0 to 10.0 in 300 steps. Corresponding elements meshing for different ka satisfies $kR(\theta)_{max} \leq 0.153$. Boundary solutions are computed with A2 based on CBIE and CHBIE, respectively. Sound pressure levels of the sample point located at $(0, 0, 1.25a)$ are plotted in Fig. 3. From Fig. 3 we observe that the A2 based on CBIE can give accurate results except at the fictitious frequencies and the A2 based on CHBIE can overcome the inaccuracy associated with the fictitious frequencies.

The CPU times used for some specific cases (not the fictitious frequencies) in the frequency sweep analysis are plotted in Fig. 4, in which the corresponding CPU times of A1 and A3 are also plotted. It further demonstrates the efficiency of the developed LF FMBEM.

5.3. Scattering from an artificial head

Generally, models in acoustic problems are more complex. In this example, we further explore the large-scale applicability of the improved LF FMBEM. A realistic artificial head model is used to test the LF FMBEM solver. The model has an overall dimension of $0.25 \times 0.43 \times 0.35$ m in x, y and z direction respectively, and is meshed with 556, 370 triangular elements. The size of the smallest triangle is 1.62×10^{-2} wavelengths, and the size of the largest one is 4.05×10^{-2} wavelengths. The maximum element number allowed in a leaf is set to 50 and 7 levels tree structure is generated. Results are compared with those given by the HF FMBEM regarding accuracy and efficiency. For the nondimensional value $ka = 96.6$ in which a is the size in y direction, the CPU time used for the LF FMBEM and HF FMBEM are 8.54 and 1.81 h, respectively. Both FMBEMs require 129 iterations to reach the solution. The boundary solutions are plotted in Fig. 5. The relative error of solutions given by the two FMBEMs is at the level of 10^{-4} which clearly demonstrated that the improved LF FMBEM can give good accuracy of acoustics problems for a wide range of frequencies. It should be noted that the rotation coefficients for multipole expansion orders larger than 30 are not correct due to the round off errors in the recurrence method. The error destroyed the accuracy of the LF FMBEM in this case. However, the recurrence method is efficient to compute the rotation coefficients. Therefore, the rotation coefficients used in the improved LF FMBEM for this case are computed with the recurrence method for multipole expansion orders less than 30 and the "pseudospectral" projection method for larger multipole expansion orders.

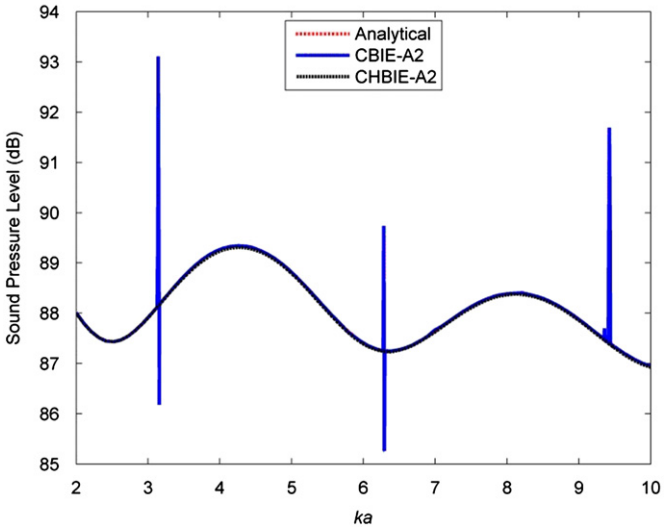

Fig. 3. Sound pressure level of the sample point computed by A1 and A2.

6. Conclusion

In this paper, an analytical integration of the hypersingular integral which is free of singular integration is adopted in the FMBEM. To compute the two regular line integrals left in the explicit hypersingular integral, analytical expressions by exploring the power series expansion of the integrands are derived. The analytical expressions just relate to the element size in wavelength regardless of the element shape. Therefore evaluations of the regular line integrals become more accurate and are easier to control the errors.

The RCR is one of the efficient algorithms for LF FMBEM. Numerical examples demonstrated that there are numerical instabilities for coefficients computed with the recurrence method. Solutions given by the LF FMBEM based on RCR with coefficients computed by the recurrence method may not accurate for higher frequency problems. Therefore the multipole expansion order should be carefully configured or other methods should be applied to compute the translation coefficients for the LF FMBEM based on the RCR. Even though the LF FMBEM based on the RCR has a complexity of $O(p^3)$ and may not give correct solutions for higher frequency acoustic problems, it still deserves investigation from the practical point of view, because it requires less memory than other FMBEMs. An improved LF FMBEM, whose moment computation and M2M translation are evaluated by the diagonal method and then the moments are translated to the LF format, is presented in this paper. The improved LF FMBEM has

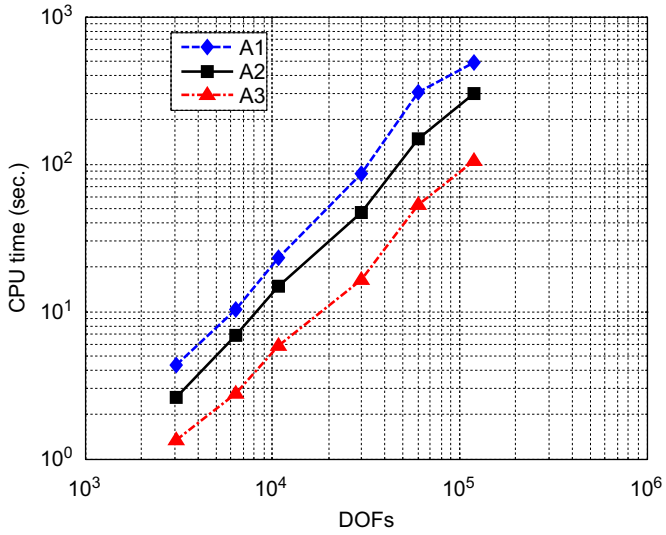

Fig. 4. CPU times used by the three FMBEMs.

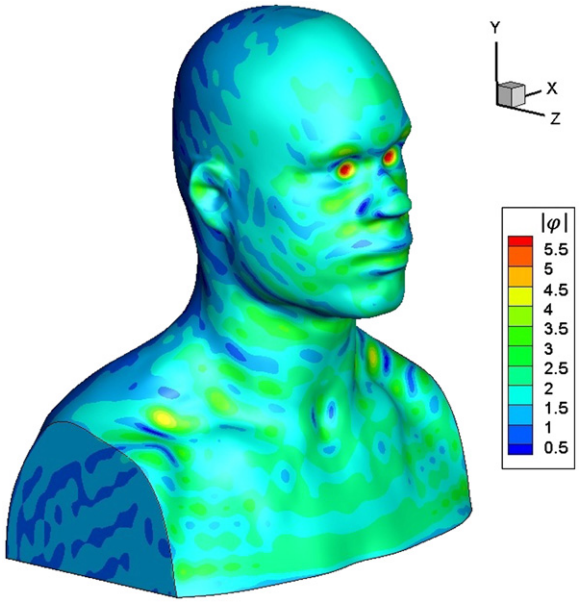

Fig. 5. Boundary solutions of an artificial head.

the same memory requirement as the one based on the RCR, and can be used for higher frequency acoustic problems. Its solution efficiency is between that of the LF FMBEM based on the RCR and that of the HF FMBEM. Numerical examples presented in this paper validate the accuracy and efficiency of the developed LF FMBEM with analytical integration of the hypersingular integral.

Acknowledgment

The work is supported by grant 11074170 of the National Natural Science Foundation of China, grant MSVMS201105 of the State Key Laboratory of Mechanical System and Vibration and the scientific foundation of graduate school of Shanghai Jiao Tong University. The authors would like to thank Mr. Shang Xiang for his help in creating the artificial head CAD model used in this study.

References

[1] Rokhlin V. Rapid solution of integral equations of classical potential theory. J Comput Phys 1985;60(2):187–207.
[2] Greengard L, Rokhlin V. A fast algorithm for particle simulations. J Comput Phys 1987;73(2):325–48.
[3] Rokhlin V. Rapid solution of integral equations of scattering theory in two dimensions. J Comput Phys 1990;86(2):414–39.
[4] Rokhlin V. Diagonal forms of translation operators for the Helmholtz equation in three dimensions. Appl Comput Harmonic Anal 1993;1(1):82–93.
[5] Epton MA, Dembart B. Multipole translation theory for the three-dimensional laplace and Helmholtz equations,. Siam J Sci Comput 1995;16(4):865–97.
[6] Rahola J. Diagonal forms of the translation operators in the fast multipole algorithm for scattering problems. BIT Numer Math 1996;36(2):333–58.
[7] Greengard L, Huang J, Rokhlin V, Wandzura S. Accelerating fast multipole methods for the Helmholtz equation at low frequencies,. IEEE Comput Sci Eng 1998;5(3):32–8.
[8] Darve E, Havé P. Efficient fast multipole method for low-frequency scattering,. J Comput Phys 2004;197(1):341–63.
[9] Sakuma T, Yasuda Y. Fast multipole boundary element method for large-scale steady-state sound field analysis. Part I: setup and validation. Acta Acust United Acust 2002;88(4):513–25.
[10] Yasuda Y, Sakuma T. Fast multipole boundary element method for large-scale steady-state sound field analysis. Part II: examination of numerical items. Acta Acust (Stuttgart) 2003;89(1):28–38.
[11] Yasuda Y, Sakuma T. An effective setting of hierarchical cell structure for the fast multipole boundary element method. J Comput Acoust 2005;13(1):47–70.
[12] Yasuda Y, Sakuma T. A technique for plane-symmetric sound field analysis in the fast multipole boundary element method. J Comput Acoust 2005;13(1):71–85.
[13] Chen JT, Chen KH. Applications of the dual integral formulation in conjunction with fast multipole method in large-scale problems for 2D exterior acoustics. Eng Anal Bound Elem 2004;28(6):685–709.
[14] Chen KH, Chen JT, Kao JH, Lee YT. Applications of the dual integral formulation in conjunction with fast multipole method to the oblique incident wave problem. Int J Numer Method Fluid 2009;59(7):711–51.
[15] Fischer M, Gauger U, Gaul L. A multipole Galerkin boundary element method for acoustics. Eng Anal Bound Elem 2004;28(2):155–62.
[16] M. Fischer, The Fast Multipole Boundary Element Method and Its Application to Structure-Acoustic Field Interaction, 2004.
[17] Fischer M, Gaul L. Application of the fast multipole bem for structural-acoustic simulations. J Comput Acoust 2005;13(1):87–98.
[18] Gaul L, Fischer M. Large-scale simulations of acoustic-structure interaction using the fast multipole BEM. ZAMM—Z Angew Math Mech 2006;86(1):4–17.
[19] Shen L, Liu YJ. An adaptive fast multipole boundary element method for three-dimensional acoustic wave problems based on the Burton–Miller formulation. Computation Mech 2007;40(3):461–72.
[20] Gumerov NA, Duraiswami R. Recursions for the computation of multipole translation and rotation coefficients for the 3-d Helmholtz equation. SIAM J Sci Comput 2003;25(4):1344–81.
[21] Bapat MS, Shen L, Liu YJ. Adaptive fast multipole boundary element method for three-dimensional half-space acoustic wave problems. Eng Anal Bound Elem 2009;33(8–9):1113–23.
[22] Bapat MS, Liu YJ. A new adaptive algorithm for the fast multipole boundary element method. CMES—Comput Modeling in Eng Sci 2010;58(2):161–83.
[23] Tong MS, Chew WC, White MJ. Multilevel fast multipole algorithm for acoustic wave scattering by truncated ground with trenches. J Acoust Soc Am 2008;123(5):2513–21.
[24] Yasuda Y, Oshima T, Sakuma T, Gunawan A, Masumoto T. Fast multipole boundary element method for low-frequency acoustic problems based on a variety of formulations. J Comput Acoust 2010;18(4):363–95.
[25] Wu HJ, Jiang WK, Liu YJ. Diagonal form fast multipole boundary element method for 2D acoustic problems based on Burton–Miller boundary integral equation formulation and its applications. Appl Math Mech (English Edition) 2011;32(8):981–96.
[26] Wu HJ, Liu YJ, Jiang WK. Analytical integration of the moments in the diagonal form fast multipole boundary element method for 3-D acoustic wave problems. Eng Anal Bound Elem 2012;36(2):248–54.
[27] Wu HJ, Jiang WK, Lu WB. Analytical moment expression for linear element in diagonal form fast multipole boundary element method. J Mech Sci Technol 2011;25(7):1711–5.
[28] Wu HJ, Liu YL, Jiang WK. A fast multipole boundary element method for 3D multi-domain acoustic scattering problems based on the Burton–Miller formulation. Eng Anal Bound Elem 2012;36(5):779–88.
[29] Cheng H, Crutchfield WY, Gimbutas Z, Greengard LF, Ethridge JF, Huang J, et al. A wideband fast multipole method for the Helmholtz equation in three dimensions. J Comput Phys 2006;216(1):300–25.
[30] Gumerov NA, Duraiswami R. A broadband fast multipole accelerated boundary element method for the three dimensional Helmholtz equation. J Acoust Soc Am 2009;125(1):191–205.
[31] Burton AJ, Miller GF. The application of integral equation methods to the numerical solution of some exterior boundary-value problems, Proceedings

of the Royal Society of London. Series A. Math Phys Sci 1971;323(1553): 201–10.
[32] Chien CC, Rajiyah H, Atluri SN. An effective method for solving the hypersingular integral equations in 3-D acoustics. J Acoust Soc Am 1990;88(2): 918–37.
[33] Liu YJ, Rizzo FJ. A weakly singular form of the hypersingular boundary integral equation applied to 3-D acoustic wave problems. Comput Method Appl Mech Eng 1992;96(2):271–87.
[34] Liu YJ, Chen SH. A new form of the hypersingular boundary integral equation for 3-D acoustics and its implementation with C0 boundary elements. Comput Method Appl Mech Eng 1999;173(3–4):375–86.
[35] Guiggiani M, Krishnasamy G, Rudolphi TJ, Rizzo FJ. A general algorithm for the numerical solution of hypersingular boundary integral equations. J Appl Mech 1992;59(3):604–14.
[36] Karami G, Derakhshan D. An efficient method to evaluate hypersingular and supersingular integrals in boundary integral equations analysis. Eng Anal Bound Elem 1999;23(4):317–26.
[37] Aimi A, Diligenti M. Hypersingular kernel integration in 3D Galerkin boundary element method. J Comput Appl Math 2002;138(1):51–72.
[38] Bonnet M, Guiggiani M. Direct evaluation of double singular integrals and new free terms in 2D (symmetric) Galerkin BEM. Comput Method Appl Mech Eng 2003;192(22–23):2565–96.
[39] Seydou F, Duraiswami R, Seppänen T, Gumerov NA. Computation of singular and hypersingular boundary integrals by Green identity and application to boundary value problems. Eng Anal Bound Elem 2009;33(8–9):1124–31.
[40] Chen K, Cheng J, Harris PJ. A new study of the Burton and Miller method for the solution of a 3D Helmholtz problem. IMA J Appl Math 2009;74(2): 163–77.
[41] Li SD, Huang QB. An improved form of the hypersingular boundary integral equation for exterior acoustic problems. Eng Anal Bound Elem 2010;34(3): 189–95.
[42] Matsumoto T, Zheng C, Harada S, Takahashi T. Explicit evaluation of hypersingular boundary integral equation for 3-d Helmholtz equation discretized with constant triangular element. J Comput Sci Technol 2010;4(3): 194–206.
[43] Zheng C, Matsumoto T, Takahashi T, Chen H. Explicit evaluation of hypersingular boundary integral equations for acoustic sensitivity analysis based on direct differentiation method. Eng Anal Bound Elem 2011;35(11):1225–35.
[44] Zheng CJ, Chen HB, Matsumoto T, Takahashi T. Three dimensional acoustic shape sensitivity analysis by means of adjoint variable method and fast multipole boundary element approach. CMES - Comput Modeling in Eng Sc 2011;79(1):1–29.
[45] Gumerov N, Duraiswami R. Fast Multipole Methods for the Helmholtz Equation in Three Dimensions. Elsevier; 2004.
[46] Ivanic J, Ruedenberg K. Rotation matrices for real spherical harmonies. direct determination by recursion. J Phys Chem 1996;100(15):6342–7.
[47] Choi CH, Ivanic J, Gordon MS, Ruedenberg K. Rapid and stable determination of rotation matrices between spherical harmonics by direct recursion. J Chem Phys 1999;111(19):8825–31.
[48] Grigoriev MM, Dargush GF. A fast multi-level boundary element method for the Helmholtz equation. Comput Method Appl Mech Eng 2004;193(3–5): 165–203.
[49] Gimbutas Z, Greengard L. A fast and stable method for rotating spherical harmonic expansions. J Comput Phys 2009;228(16):5621–7.
[50] Coifman R, Rokhlin V, Wandzura S. The fast multipole method for the wave equation: a pedestrian prescription. IEEE Antennas Propag Mag 1993;35(3): 7–12.